


**Spin Hall effect: Symmetry breaking, twisting, and giant disorder renormalization**David T. S. Perkins <sup>\*</sup>, Alessandro Veneri <sup>\*</sup>, and Aires Ferreira <sup>†</sup>*School of Physics, Engineering and Technology and York Centre for Quantum Technologies,  
University of York, YO10 5DD York, United Kingdom*

(Received 21 March 2024; revised 31 May 2024; accepted 4 June 2024; published 17 June 2024)

Atomically thin materials based on transition-metal dichalcogenides and graphene offer a promising avenue for unlocking the mechanisms underlying the spin Hall effect (SHE) in heterointerfaces. Here we develop a microscopic theory of the SHE for twisted van der Waals heterostructures that fully incorporates twisting and disorder effects and illustrate the critical role of symmetry breaking in the generation of spin Hall currents. We find that an accurate treatment of vertex corrections leads to a qualitatively and quantitatively different SHE than that obtained from the popular  $i\eta$  and ladder approximations. A pronounced oscillatory behavior of skew-scattering processes with twist angle  $\theta$  is predicted, reflecting a nontrivial interplay of Rashba and valley-Zeeman effects and yields a vanishing SHE for  $\theta = 30^\circ$  and, for graphene-WSe<sub>2</sub> heterostructures, an optimal SHE for  $\theta \approx 17^\circ$ . Our findings reveal disorder and broken symmetries as important knobs to optimize interfacial SHEs.

DOI: [10.1103/PhysRevB.109.L241404](https://doi.org/10.1103/PhysRevB.109.L241404)

*Introduction.* The discovery of superconductivity [1,2], flat bands [3–6], strongly correlated insulating phases, and topological behavior [7,8] in layer-twisted honeycomb systems has led them to be at the center of many theoretical and experimental studies [9–20]. The significance of twisting in the plethora of spin-dependent phenomena generated by spin-orbit coupling (SOC) is currently under intense investigation [21–29]. It has been shown that the modification of the Fermi surface’s spin texture induced by twisting [21–25] leads to profound changes in the spin-charge interconversion processes displayed by graphene–transition-metal dichalcogenide (TMD) bilayers [26,27], a paradigmatic system in the burgeoning field of graphene spintronics [30–32]. Despite these advances, a microscopic theory of the spin Hall effect (SHE), i.e., the generation of a transverse spin current due to an applied electric field, reflective of the untwisted, let alone twisted, van der Waals (vdW) heterostructures used in spin Hall experiments [33–41], remains an elusive task. Such a theory could offer valuable insight into the role of broken spatial symmetry and relative atomic orientation between layers. Through twisting, the single unique mirror plane present in aligned graphene-TMD bilayers is lost, reducing the symmetry from  $C_{3v}$  to the chiral point group  $C_3$ . From a physical perspective, the metal-chalcogen environment around each carbon atom is changed as the layers are twisted, leading to

a modulation of the out-of-plane asymmetry SOC (Rashba effect) and the sublattice-resolved SOC (valley-Zeeman effect). Twisted vdW heterostructures therefore provide a natural, highly tunable platform to investigate interfacial SHEs and may serve as a guide in examining other heterointerfaces.

Another key question is the breaking of translation symmetry due to disorder, which is known to profoundly modify the electrodynamic response of spin-orbit-coupled Dirac bands [32]. The ubiquitous nature of disorder in two-dimensional (2D) crystals makes it a crucial ingredient for understanding both the SHE and the wealth of magneto-electric effects underlying charge-to-spin conversion, such as the inverse spin galvanic effect (ISGE). The ISGE has been understood in both untwisted [42,43] and twisted [26] 2D vdW heterostructures with dilute random impurities. In contrast, previous theoretical work on the SHE has focused on minimal models of proximitized graphene, i.e., without disorder [44,45], within the Rashba spin gap [46], and in the absence of the valley-Zeeman effect [47]. The diffusive SHE with a Fermi energy located well above the spin gap, the most experimentally accessible and well controlled regime due to the suppression of carrier-density inhomogeneities [33–41], is theoretically challenging, and more so for comprehensive graphene-TMD models with competing symmetry-breaking effects. Unlike the conventional ISGE, where the nonequilibrium spin density is simply proportional to the charge transport time, the extrinsic SHE is governed by its own timescales (which, technically speaking, are encoded in vertex corrections to spin-charge response functions). The microscopic processes governing the SHE reflect the rich interplay between Fermi-surface spin texture (quantum geometry) and spin-orbit scattering mechanisms (extrinsic effects) and hence constitute a critical puzzle piece in understanding nonlocal spin transport experiments [36,37] as well as guiding future efforts in spin

<sup>\*</sup>Contact author: david.t.s.perkins@york.ac.uk<sup>†</sup>Contact author: aires.ferreira@york.ac.uk

twistronics. While real-space techniques for billion-atom calculations of linear response functions have recently been devised that could in principle be used to overcome the aforementioned challenges [48–50], the scarce numerical studies of the SHE in the literature simulated small systems (of order 10 nm in linear size, i.e., quantum-dot territory [51]) and hence are far from capturing the transport regimes seen in experiments.

In this Letter, we construct a microscopic theory for twisted graphene-TMD systems that accounts for band structure effects nonperturbatively and straddles strong- and weak-scattering regimes, hence overcoming the above challenges via a unified approach. The most surprising result is a giant modulation of the spin Hall conductivity with twist angle, yielding an optimal SHE for chiral bilayers at a critical twist angle ( $\theta_c \approx 17^\circ$  for graphene-WSe<sub>2</sub> heterostructures). This novel behavior, reflective of the sensitivity of disorder corrections to quantum-geometric effects, is absent in the  $i\eta$  approximation. Moreover, our findings suggest that purely diffusive SHEs in graphene-TMD systems are dominated by skew-scattering processes with large cross sections. An intriguing exception are  $C_{3v}$ -invariant systems with  $\theta = 30^\circ$ . Here anomalous scattering processes due to spatial fluctuations of the proximity-induced SOCs [52–54] are expected to govern the steady-state SHE.

*Model and theory.* We implement the Hamiltonian of Refs. [21–26] for the low-energy graphene-TMD description, which assumes the axes to be taken in the graphene sheet’s frame of reference. Specifically ( $\hbar = 1$ ), for the clean system we write  $H_{\mathbf{k}} = H_{0\mathbf{k}} + H_R + H_{VZ}$  ( $\mathbf{k}$  is the wave vector measured from a Dirac point), with  $H_{0\mathbf{k}} = v(\tau_z \sigma_x k_x + \sigma_y k_y)$ ,  $H_{VZ} = \lambda_{VZ}(\theta) \tau_z s_z$ , and

$$H_R = \lambda_R(\theta) e^{is_z[\alpha_R(\theta)/2]} (\tau_z \sigma_x s_y - \sigma_y s_x) e^{-is_z[\alpha_R(\theta)/2]}, \quad (1)$$

where  $\lambda_R(\theta)$ ,  $\alpha_R(\theta)$ , and  $\lambda_{VZ}(\theta)$  are the twist-dependent Rashba magnitude, Rashba phase, and valley-Zeeman coupling, respectively;  $v$  is the bare Fermi velocity; and  $\tau_i$ ,  $\sigma_i$ , and  $s_i$  ( $i \in \{x, y, z\}$ ) are the Pauli matrices acting on the valley, sublattice, and spin degrees of freedom, respectively. Here we use the  $\theta$  dependence of the SOC magnitudes accurately mapped by recent quantum interference measurements on twisted graphene-WSe<sub>2</sub> heterostructures [28] to predict the full  $\theta$  dependence of the SHE. Furthermore, we include scalar disorder in our model via the term  $V(\mathbf{r}) = \sum_i u_0 \delta(\mathbf{r} - \mathbf{R}_i)$ , where  $\{\mathbf{R}_i\}$  is the set of impurity positions and  $u_0$  characterizes the impurity scattering strength. Short-range disorder typically dominates the electronic transport when probing behavior away from the charge neutrality point [55–57] (thus electron-hole puddles are expected to play no role in the transport physics located above the Rashba gap). We further note that the twisted bilayer system under study generally belongs to the  $C_3$  chiral group, except for the discrete set of twist angles  $\theta = p\pi/3$  ( $p \in \mathbb{Z}$ ), at which the symmetry is elevated to  $C_{3v}$  due to the presence of a mirror plane. Moreover, as shown below, there is an important hidden symmetry for  $\theta = \pi/6$ . These considerations will become crucial when assessing the disorder corrections to SHE.

The spin Hall conductivity  $\sigma^{\text{SH}}$  is calculated from the Kubo-Streda formula [54,58,59] using an extension of the

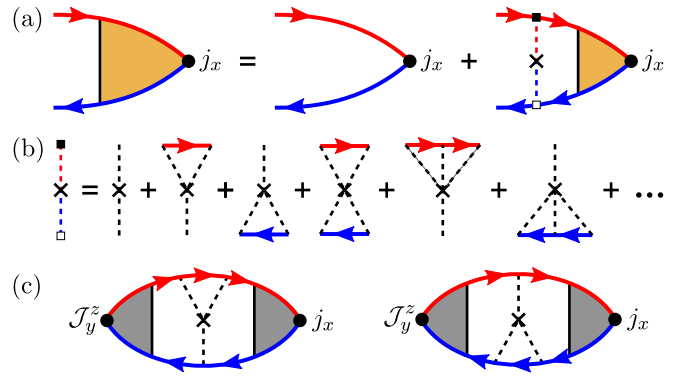


FIG. 1. (a) Renormalized charge current vertex within the  $T$ -matrix formalism. Red (blue) solid lines denote disorder-averaged retarded (advanced) Green’s functions, red (blue) dashed lines with black (white) boxes represent retarded (advanced)  $T$  matrices, and the black cross signifies the insertion of the scalar impurity density. (b) Expansion of the  $T$ -matrix vertex renormalization. The black dashed lines denotes an impurity scattering event. (c)  $Y$  diagrams showing the response functions with the insertion of a single third-order scattering event. The gray shading indicates the renormalization of the vertices within the BA [retaining only the first term in (b)].

$T$ -matrix diagrammatic technique of Ref. [54] to spin-orbit-coupled bands. The transport in the dilute impurity regime is governed by the Fermi-surface contribution

$$\sigma^{\text{SH}} = \sum_{\mathbf{k}} \text{tr}(\mathcal{J}_y^z \mathcal{G}_{\mathbf{k}}^+ \tilde{j}_x \mathcal{G}_{\mathbf{k}}^-), \quad (2)$$

where  $\mathcal{G}_{\mathbf{k}}^{\pm} = (G_{0,\mathbf{k}}^{\pm-1} - \Sigma^{\pm})^{-1}$  are the disorder-averaged retarded (+) and advanced (–) Green’s functions at the Fermi energy  $\varepsilon$ ,  $\Sigma^{\pm}$  are the disorder self-energies,  $G_{0,\mathbf{k}}^{\pm} = (\varepsilon - H_{\mathbf{k}} \pm i0^+)^{-1}$  are the clean Green’s functions,  $\mathcal{J}_y^z = v\sigma_y s_z/2$  is the spin current operator,  $j_x = -e\partial_k H_{\mathbf{k}}$  is the charge current operator in the  $x$  direction ( $e > 0$ ),  $\tilde{j}_x$  is the disorder-renormalized charge current operator (Fig. 1), and the trace is taken over all internal degrees of freedom. Equation (2) captures all possible single-impurity scattering processes when handled within the  $T$ -matrix formalism outlined in Figs. 1(a) and 1(b). Most notably it accounts for skew-scattering (semiclassical) and side-jump (quantum) corrections in a fully nonperturbative fashion [54]. If vertex corrections are ignored,  $\sigma^{\text{SH}}$  fails to vanish when  $\lambda_{VZ} = 0$ , thus violating the exact  $SU(2)$ -gauge covariance of the Rashba-coupled system [60,61]. As it turns out, vertex corrections are also essential when sublattice symmetry is broken, i.e.,  $\lambda_{VZ} = \lambda_A - \lambda_B \neq 0$  [32], where  $\lambda_{A(B)}$  is the intrinsic SOC on  $A$  ( $B$ ) sites. We demonstrate this in two complementary ways: by means of a numerical evaluation of the  $T$ -matrix series (full resummation) and an analytical calculation of a subset of Feynman diagrams. The latter provides insights into the microscopic mechanisms governing the SHE, while the former allows us to reach the strong- and unitary scattering regimes, e.g., describing resonant impurities [62].

*Results.* We specialize to the case  $|\varepsilon| > \Delta_s$ , where  $\Delta_s = \sqrt{4\lambda_R^2 + \lambda_{VZ}^2}$  is the spin gap, which, as mentioned previously,

is the most pertinent parameter region. We start by describing the impact of skew scattering to leading order in  $u_0$ . This is achieved by calculating the  $Y$  diagrams shown in Fig. 1(c), in which the Green's functions and vertices are renormalized within the first Born approximation (BA),

$$\sigma_Y^{\text{SH}} = \sum_{\mathbf{k}, \mathbf{p}} 2 \operatorname{Re}[\operatorname{tr}[\mathcal{G}_{\mathbf{k}}^- \tilde{\mathcal{J}}_y^z \mathcal{G}_{\mathbf{k}}^+ Y^+ \mathcal{G}_{\mathbf{p}}^+ \tilde{\mathcal{J}}_x \mathcal{G}_{\mathbf{p}}^-]], \quad (3)$$

where  $Y^+ = nu_0^3 \sum_{\mathbf{q}} \mathcal{G}_{\mathbf{q}}^+$  is the retarded skew-scattering insertion,  $\mathcal{G}_{\mathbf{k}}^{\pm}$  are the Green's functions evaluated within the BA, and  $\tilde{\mathcal{J}}_y^z$  and  $\tilde{\mathcal{J}}_x$  are the disorder-renormalized spin current and charge current vertices, respectively, calculated within the BA. We note that the Rashba phases in Eq. (1) can be removed by untwisting the full Hamiltonian via a unitary spin rotation (see Ref. [26] for details).

Evaluating the  $Y$  diagrams in Fig. 1 produces

$$\sigma_Y^{\text{SH}} = \frac{2e\varepsilon}{n\pi u_0} \frac{\lambda_{\text{R}}^4 \lambda_{\text{vZ}}^2 (\varepsilon^2 - \lambda_{\text{vZ}}^2) (\varepsilon^2 + \lambda_{\text{vZ}}^2)^2}{[\varepsilon^4 (\lambda_{\text{R}}^2 + \lambda_{\text{vZ}}^2) + 3\lambda_{\text{R}}^2 \lambda_{\text{vZ}}^4 - \varepsilon^2 \lambda_{\text{vZ}}^4]^2} \quad (4)$$

to leading order  $O(n^{-1})$  in the impurity concentration. The intricate behavior with the Fermi energy and  $\theta$ -dependent SOCs encoded in Eq. (4) reflects a remarkable reliance of disorder effects on the spin-orbital texture of Bloch wave functions (the quantum geometry of energy bands [42]). Principally, a noncoplanar Rashba spin texture (and thus  $\lambda_{\text{vZ}} \neq 0$ ) is required for a nonvanishing SHE. This has a simple interpretation: Skew scattering from scalar impurities relies upon electronic states with a well-defined spin polarization around a valley to enable a clear separation between spin-up and spin-down scattering channels. The tilted Rashba spin textures in graphene-TMD systems generally satisfy this requirement. Thus, a spin Hall response naturally emerges when the sublattice symmetry is broken [note that  $\lambda_{\text{R}}(\theta)$  is guaranteed to be nonzero due to the interfacial breaking of the horizontal mirror plane]. These considerations remains true at  $O(n^0)$ , further emphasizing the critical role played by vertex corrections. In addition to occurring at  $O(n^{-1})$ , the renormalized response also carries a factor of  $u_0^{-1}$ , which puts it at the next order in the scattering strength when compared to the electrical conductivity and spin susceptibility [26,47]. Anomalous scattering processes, such as single-impurity side jumps and diffractive skew scattering [54,63–65], kick in to next order in the small- $n$  expansion and thus are relevant for samples with low carrier mobility. They are not considered here.

We now turn to the nonperturbative results in the scattering strength obtained by resumming the infinite  $T$ -matrix series in Fig. 1(b) numerically. The range of impurity concentrations we focus on is chosen to yield bona fide diffusive spin transport, i.e.,  $\sigma^{\text{SH}} \sim n^{-1}$ . The valley-Zeeman behavior of the steady-state spin Hall conductivity and spin Hall angle,  $\theta_{\text{SH}} = 2e\sigma^{\text{SH}}/\sigma_{\text{xx}}$ , is shown in Fig. 2 in both the weak-scattering and unitary limits. (For consistency, we calculate the charge conductivity  $\sigma_{\text{xx}}$  from linear response theory with the same methodology used for  $\sigma^{\text{SH}}$ .) Moreover, the weak-scattering limit of  $\sigma^{\text{SH}}$  (solid line) is obtained via Eq. (4); a numerical calculation in this regime is out of reach due to the smallness of the disorder self-energy. We see that while the weak-scattering limit may yield a nominally large

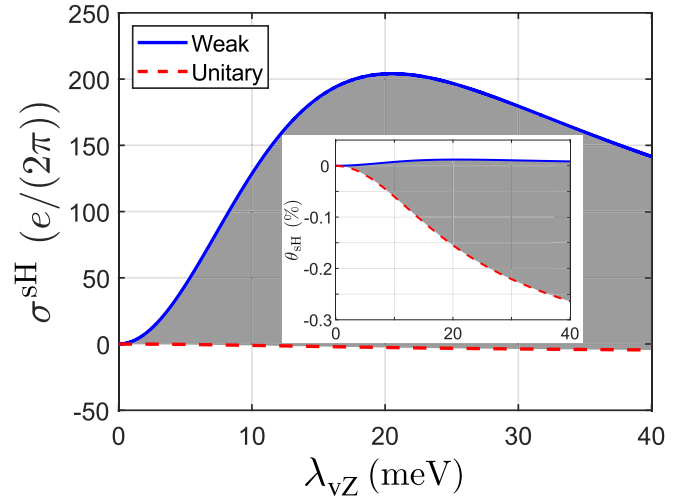


FIG. 2. Valley-Zeeman coupling dependence of the spin Hall response for weak-scattering potentials [Eq. (4), with  $u_0 = 0.1$  eV nm<sup>2</sup>] and unitary ( $u_0 \rightarrow \infty$ ) limits. A fixed Fermi energy of  $\varepsilon = 0.2$  eV is assumed along with  $n = 10^{14}$  m<sup>-2</sup> and  $\lambda_{\text{R}} = 20$  meV. The gray region is the area accessible with intermediate-scattering strengths. The inset shows the same plot but for the spin Hall angle  $\theta_{\text{SH}}$ .

magnitude of the spin Hall response, the corresponding spin-charge conversion efficiency is significantly lower than in the unitary case ( $|\theta_{\text{SH}}^{\text{unitary}}| \gg |\theta_{\text{SH}}^{\text{weak}}|$ ). This can be inferred from the scaling behaviors in the perturbative regime,  $\sigma^{\text{SH}} \propto u_0^{-1}$  [see Eq. (4)], as opposed to the faster decay featured by the electrical conductivity ( $\sigma_{\text{xx}} \propto u_0^{-2}$ ). Furthermore, the charge transport coefficients have distinct Fermi energy dependences in the Born and unitary scattering regimes. Specifically,  $\sigma_{\text{xx}} \sim \varepsilon^0$  (BA) and  $\sigma_{\text{xx}} \sim \varepsilon^2$  (unitary) in the limit  $\varepsilon \gg \Delta_s$ . This is fortunate, because the measured charge conductivity in graphene-TMD systems closely follows the  $\varepsilon^2$  law in the intermediate- to high-charge-carrier-density regime [39,66], thus matching the results of our theory in the unitary limit and hence evidencing its predictive power. In this strong-scattering regime, not only do the predicted spin Hall angles reach detectable values (see inset in Fig. 2), more importantly, they agree well with lateral spin Hall measurements [39]. Additionally,  $|\sigma^{\text{SH}}|$  increases with  $\lambda_{\text{vZ}}$  in a monotonic fashion for strong disorder, exhibiting no turning points inside a reasonable range of  $\lambda_{\text{vZ}}$ , unlike the weak-scattering response, which displays a maximum at  $\lambda_{\text{vZ}} \simeq \lambda_{\text{R}}$ .

The considerations above show that the unitary scattering regime should be the primary focus when analyzing the SHE of realistic systems. To this end, we use the twist-dependent SOC magnitudes  $\lambda_{\text{R}}(\theta)$  and  $\lambda_{\text{vZ}}(\theta)$  probed in recent experiments on graphene-WSe<sub>2</sub> heterostructures [28]. To extrapolate the experimental data to twist angles greater than  $\pi/6$ , we exploit the twist angle symmetries of the individual SOCs [22,23]. In practice, this is accomplished by fitting a minimal Fourier series to the data of Ref. [28] [see Figs. 3(b) and 3(c)]. To further improve the accuracy of our results, we also account for the SU(2) gauge covariance breaking due to the momentum cutoff regularization ( $k_{\text{max}} = \Lambda/v$ , where  $\Lambda$  is the energy cutoff) of our numerical

scheme [67]. The ensuing twist angle behavior of the spin Hall response in the unitary limit is shown in Fig. 3(a), which is the main finding of this Letter. The significance of these results is best appreciated by a direct comparison against the  $i\eta$ -approximated response  $\sigma_\eta^{\text{SH}}$ , wherein  $\Sigma^\pm = \mp i\eta$  and vertex corrections are neglected [67]. We immediately see that  $\sigma^{\text{SH}}$  and  $\sigma_\eta^{\text{SH}}$  differ in several ways. Most importantly,  $\sigma^{\text{SH}}$  vanishes when  $\lambda_{\text{vz}} = 0$ , while  $\sigma_\eta^{\text{SH}}$  reaches a maximal value at this point. Furthermore, the  $i\eta$  approximation yields a response that is not only different in sign, but also an order of magnitude larger than the renormalized result. We glean insight for this size discrepancy from the weak-scattering limit, where  $\sigma^{\text{SH}} \sim \varepsilon^{-1}$  for large Fermi energies in contrast to  $\sigma_\eta^{\text{SH}}$  tending towards some constant value [67]. The  $i\eta$  scheme irrefutably fails in modeling the SHE, even when accounting for the parametric dependences of the broadening  $\eta = \eta(\theta)$ . Finally, we note that the ladder approximation, corresponding to only considering the first diagram in the skeleton expansion of Fig. 1(b), also fails to describe the giant skew-scattering-driven SHE modulation reported here. This is because the left-right asymmetry of scattering cross sections manifests at third order in the scattering potential, as is well known. Before discussing twisting effects, a cautionary remark is in order: Short-range defects generate substantial valley mixing [55–57], which is absent in our disorder model. Because the skew cross section has opposite signs in the  $K$  and  $K'$  valleys (courtesy of the valley-Zeeman effect), intervalley scattering events diminish the skewness of spin-up/spin-down scattering channels and thus the spin Hall conductivity [68]. Given the prominence of band-driven skew scattering in graphene-based heterostructures [61], the use of interfaces free of atomic defects is advisable to fully exploit the advantages of proximity-induced SOC for the SHE. For a quantitative analysis of the interplay of intervalley and skew scattering in honeycomb layered systems, we refer the reader to Refs. [61,68], where these ideas were first discussed.

*Twisting effects.* We first focus on the region of twist angles close to  $30^\circ$  as this will be the area hosting the most exotic physics (Fig. 3). At  $\theta = 30^\circ$ , the graphene-TMD system has  $C_{3v}$  symmetry, akin to untwisted bilayers. However, unlike perfectly aligned heterostructures, there is a hidden sublattice symmetry in our continuum model. This is because  $\lambda_{\text{vz}}(30^\circ) = 0$  and thus the clean system possesses chiral (sublattice) symmetry [69] at zero chemical potential,  $\sigma_z H_{\mathbf{k}} \sigma_z = -H_{\mathbf{k}}$ . (We note that our model omits a small sublattice-resolved scalar potential effects in accord with perturbation theory [22] and first-principles calculations [25].) As such, we speculate that, when the twist angle is equal or close to  $30^\circ$ , small fluctuations in the proximity-induced spin-orbit fields will dominate the SHE due to  $\lambda_{\text{vz}}$  approaching zero. These fluctuations can arise from ripples in the graphene flake [70] and nonuniform twisting across the sample [71]. Both of these will yield spatially varying spin-orbit couplings that can engender anomalous spin Hall responses [52,53]. The exact consequence of these fluctuations makes for an interesting question for further study beyond this work. Second, we see that the spin Hall response in WSe<sub>2</sub> is optimal for  $\theta \approx 17^\circ$ , by virtue of the maximal value of  $|\lambda_{\text{vz}}(\theta)|$ . The strong

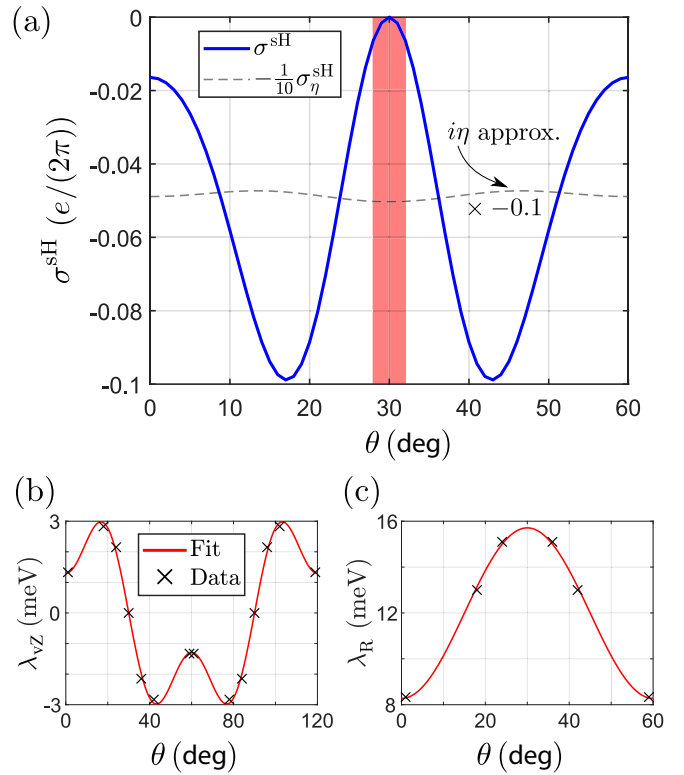


FIG. 3. (a) Twist angle dependence for the renormalized and  $i\eta$ -approximated spin Hall conductivities for a graphene-WSe<sub>2</sub> bilayer based on the experimental observations of Ref. [28], within the unitary and diffusive limits. The shaded region indicates where quantum effects will play a major role. Here we take  $\varepsilon = 0.2$  eV,  $n = 10^{14}$  m<sup>-2</sup>, and  $\Lambda = 10$  eV. (b) and (c) Minimal Fourier series fits to the experimental data (black crosses) of Ref. [28].

modulation of  $\sigma^{\text{SH}}$  demonstrated here is a direct indicator of the giant renormalization generated by the interplay of disorder and twist-dependent Fermi surface spin texture. In closing this discussion, we finally note that changing the TMD of this heterostructure will naturally yield a different twist angle dependence of the spin Hall conductivity and angle. The resulting change cannot be predicted through intuition alone and may be drastic, as hinted at by the difference in twist angle variation of the SOC strengths shown in Ref. [23]. The only guaranteed similarity is the vanishing of  $\sigma^{\text{SH}}$  at  $\theta = 30^\circ$ .

*Lateral spin transport.* Finally, we frame our results in the context of recent experiments detecting the SHE in graphene-TMD systems using spin precession techniques in Hall bar geometry [37,39]. Within the weak-scattering regime [specifically,  $u_0 \ll \nu_0(\varepsilon)^{-1}$ , with  $\nu_0(\varepsilon)$  the clean density of states], the observed spin Hall angles ( $\theta_{\text{SHE}}^{\text{exp}} \sim 0.1\text{--}1\%$ ) are not achievable, even with proximity-induced SOC choices larger than that recently mapped out by quantum interference imaging [28]. Our microscopic theory predicts  $\theta_{\text{SHE}} \sim 0.02\%$  for  $\lambda_{\text{R}} = \lambda_{\text{vz}} = 20$  meV (see Fig. 2), indicating that the behavior observed in spin Hall transport experiments is the result of strong-scattering potentials. Working in the unitary limit, we find that a spin Hall angle of order 0.1% is achievable with larger SOC strengths or at higher impurity concentrations (approximately  $5 \times 10^{15}$  m<sup>-2</sup>); however, this starts to move the

system away from the diffusive limit. For example, for a system reflective of graphene-WSe<sub>2</sub> heterostructures [28,29] ( $\lambda_R = 14$  meV and  $\lambda_{VZ} = 3$  meV) with  $n = 4.5 \times 10^{15} \text{m}^{-2}$ , we obtain  $\theta_{\text{SHE}} = 0.11\%$  and find  $\sigma_{xx}$  to be approximately diffusive [ $\sigma_{xx}(n)/\sigma_{xx}(2n) = 2.3$ ]. However, the  $\sigma^{\text{SH}}$  calculated within the  $T$ -matrix method turns out to be nondiffusive, reflecting higher-order corrections in  $n$ . Given the breakdown of the diffusive limit in obtaining spin Hall angles comparable to experiment, our findings suggest that bona fide quantum effects, such as diffractive skew scattering described by crossing diagrams [54], may play a role in the spin transport observed.

*Conclusion.* Our work has demonstrated the necessity for vertex corrections in the accurate modeling of the SHE in lay-

ered materials with competing broken symmetries. We found that disorder impacts pure interfacial SHEs in an unexpected way, leading to a strong oscillatory behavior of the spin Hall response upon twisting. The twist angle dependence of the SHE uncovered here reflects the underlying quantum geometry of electronic states in regions of noncoplanar spin texture and allows for the regimes in which spatial fluctuations and intrinsic effects may dominate, thus raising intriguing questions for future research.

*Acknowledgments.* D.T.S.P., A.V., and A.F. acknowledge support from the Royal Society through Grants No. URF\R191021, No. RFA\ERE\210281, and No. RGF\EA\180276.

- 
- [1] Y. Cao, V. Fatemi, S. Fang, K. Watanabe, T. Taniguchi, E. Kaxiras, and P. Jarillo-Herrero, Unconventional superconductivity in magic-angle graphene superlattices, *Nature (London)* **556**, 43 (2018).
- [2] H. Isobe, N. F. Q. Yuan, and L. Fu, Unconventional superconductivity and density waves in twisted bilayer graphene, *Phys. Rev. X* **8**, 041041 (2018).
- [3] S. Shallcross, S. Sharma, E. Kandelaki, and O. A. Pankratov, Electronic structure of turbostratic graphene, *Phys. Rev. B* **81**, 165105 (2010).
- [4] R. Bistritzer and A. H. MacDonald, Moiré bands in twisted double-layer graphene, *Proc. Natl. Acad. Sci. USA* **108**, 12233 (2011).
- [5] G. Trambly de Laissardière, D. Mayou, and L. Magaud, Numerical studies of confined states in rotated bilayers of graphene, *Phys. Rev. B* **86**, 125413 (2012).
- [6] P. Moon and M. Koshino, Energy spectrum and quantum Hall effect in twisted bilayer graphene, *Phys. Rev. B* **85**, 195458 (2012).
- [7] A. K. Geim and I. V. Grigorieva, Van der Waals heterostructures, *Nature (London)* **499**, 419 (2013).
- [8] K. S. Novoselov, A. Mishchenko, A. Carvalho, and A. H. C. Neto, 2D materials and van der Waals heterostructures, *Science* **353**, aac9439 (2016).
- [9] L. Zou, H. C. Po, A. Vishwanath, and T. Senthil, Band structure of twisted bilayer graphene: Emergent symmetries, commensurate approximants, and Wannier obstructions, *Phys. Rev. B* **98**, 085435 (2018).
- [10] Y. Choi, J. Kemmer, Y. Peng, A. Thomson, H. Arora, R. Polski, Y. Zhang, H. Ren, J. Alicea, G. Refael *et al.*, Electronic correlations in twisted bilayer graphene near the magic angle, *Nature (London)* **15**, 1174 (2019).
- [11] L. Classen, C. Honerkamp, and M. M. Scherer, Competing phases of interacting electrons on triangular lattices in moiré heterostructures, *Phys. Rev. B* **99**, 195120 (2019).
- [12] X. Lu, P. Stepanov, W. Yang, M. Xie, M. A. Aamir, I. Das, C. Urgell, K. Watanabe, T. Taniguchi, G. Zhang *et al.*, Superconductors, orbital magnets and correlated states in magic-angle bilayer graphene, *Nature (London)* **574**, 653 (2019).
- [13] B. Lian, Z. Wang, and B. A. Bernevig, Twisted bilayer graphene: A phonon-driven superconductor, *Phys. Rev. Lett.* **122**, 257002 (2019).
- [14] G. Tarnopolsky, A. J. Kruchkov, and A. Vishwanath, Origin of magic angles in twisted bilayer graphene, *Phys. Rev. Lett.* **122**, 106405 (2019).
- [15] M. Yankowitz, S. Chen, H. Polshyn, Y. Zhang, K. Watanabe, T. Taniguchi, D. Graf, A. F. Young, and C. R. Dean, Tuning superconductivity in twisted bilayer graphene, *Science* **363**, 1059 (2019).
- [16] Y. Cao, D. Chowdhury, D. Rodan-Legrain, O. Rubies-Bigorda, K. Watanabe, T. Taniguchi, T. Senthil, and P. Jarillo-Herrero, Strange metal in magic-angle graphene with near Planckian dissipation, *Phys. Rev. Lett.* **124**, 076801 (2020).
- [17] B. Padhi, A. Tiwari, T. Neupert, and S. Ryu, Transport across twist angle domains in moiré graphene, *Phys. Rev. Res.* **2**, 033458 (2020).
- [18] Y. D. Liao, J. Kang, C. N. Breið, X. Y. Xu, H.-Q. Wu, B. M. Andersen, R. M. Fernandes, and Z. Y. Meng, Correlation-induced insulating topological phases at charge neutrality in twisted bilayer graphene, *Phys. Rev. X* **11**, 011014 (2021).
- [19] Z.-D. Song and B. A. Bernevig, Magic-angle twisted bilayer graphene as a topological heavy fermion problem, *Phys. Rev. Lett.* **129**, 047601 (2022).
- [20] J. Duan, Y. Jian, Y. Gao, H. Peng, J. Zhong, Q. Feng, J. Mao, and Y. Yao, Giant second-order nonlinear Hall effect in twisted bilayer graphene, *Phys. Rev. Lett.* **129**, 186801 (2022).
- [21] Y. Li and M. Koshino, Twist-angle dependence of the proximity spin-orbit coupling in graphene on transition-metal dichalcogenides, *Phys. Rev. B* **99**, 075438 (2019).
- [22] A. David, P. Rakyta, A. Kormányos, and G. Burkard, Induced spin-orbit coupling in twisted graphene-transition metal dichalcogenide heterobilayers: Twistronics meets spintronics, *Phys. Rev. B* **100**, 085412 (2019).
- [23] C. G. Péterfalvi, A. David, P. Rakyta, G. Burkard, and A. Kormányos, Quantum interference tuning of spin-orbit coupling in twisted van der Waals trilayers, *Phys. Rev. Res.* **4**, L022049 (2022).
- [24] A. Pezo, Z. Zanolli, N. Wittemeier, P. Ordejón, A. Fazzio, S. Roche, and J. H. Garcia, Manipulation of spin transport in graphene/transition metal dichalcogenide heterobilayers upon twisting, *2D Mater.* **9**, 015008 (2022).
- [25] T. Naimier, K. Zollner, M. Gmitra, and J. Fabian, Twist-angle dependent proximity induced spin-orbit coupling in

- graphene/transition metal dichalcogenide heterostructures, *Phys. Rev. B* **104**, 195156 (2021).
- [26] A. Veneri, D. T. S. Perkins, C. G. Péterfalvi, and A. Ferreira, Twist angle controlled collinear Edelstein effect in van der Waals heterostructures, *Phys. Rev. B* **106**, L081406 (2022).
- [27] S. Lee, D. J. P. de Sousa, Y.-K. Kwon, F. de Juan, Z. Chi, F. Casanova, and T. Low, Charge-to-spin conversion in twisted graphene/WSe<sub>2</sub> heterostructures, *Phys. Rev. B* **106**, 165420 (2022).
- [28] L. Sun, L. Rademaker, D. Mauro, A. Scarfato, Á. Pásztor, I. Gutiérrez-Lezama, Z. Wang, J. Martínez-Castro, A. F. Morpurgo, and C. Renner, Determining spin-orbit coupling in graphene by quasiparticle interference imaging, *Nat. Commun.* **14**, 3771 (2023).
- [29] Q. Rao, W.-H. Kang, H. Xue, Z. Ye, X. Feng, K. Watanabe, T. Taniguchi, N. Wang, M.-H. Liu, and D.-K. Ki, Ballistic transport spectroscopy of spin-orbit-coupled bands in monolayer graphene on WSe<sub>2</sub>, *Nat. Commun.* **14**, 6124 (2023).
- [30] A. Avsar, H. Ochoa, F. Guinea, B. Özyilmaz, B. J. van Wees, and I. J. Vera-Marun, *Colloquium: Spintronics in graphene and other two-dimensional materials*, *Rev. Mod. Phys.* **92**, 021003 (2020).
- [31] J. F. Sierra, J. Fabian, R. K. Kawakami, S. Roche, and S. O. Valenzuela, Van der Waals heterostructures for spintronics and opto-spintronics, *Nat. Nanotechnol.* **16**, 856 (2021).
- [32] D. Perkins and A. Ferreira, in *Encyclopedia of Condensed Matter Physics*, 2nd ed., edited by T. Chakraborty (Academic, Oxford, 2024), pp. 205–222.
- [33] A. Avsar, J. Y. Tan, T. Taychatanapat, J. Balakrishnan, G. K. W. Koon, Y. Yeo, J. Lahiri, A. Carvalho, A. S. Rodin, E.C.T. O'Farrell *et al.*, Spin-orbit proximity effect in graphene, *Nat. Commun.* **5**, 4875 (2014).
- [34] Z. Wang, D.-K. Ki, H. Chen, H. Berger, A. H. MacDonald, and A. F. Morpurgo, Strong interface-induced spin-orbit interaction in graphene on WS<sub>2</sub>, *Nat. Commun.* **6**, 8339 (2015).
- [35] T. S. Ghiasi, J. Ingla-Aynés, A. A. Kaverzin, and B. J. van Wees, Large proximity-induced spin lifetime anisotropy in transition-metal dichalcogenide/graphene heterostructures, *Nano Lett.* **17**, 7528 (2017).
- [36] L. A. Benítez, J. F. Sierra, W. Savero Torres, A. Arighi, F. Bonell, M. V. Costache, and S. O. Valenzuela, Strongly anisotropic spin relaxation in graphene–transition metal dichalcogenide heterostructures at room temperature, *Nat. Phys.* **14**, 303 (2018).
- [37] C. K. Safeer, J. Ingla-Aynés, F. Herling, J. H. Garcia, M. Vila, N. Ontoso, M. R. Calvo, S. Roche, L. E. Hueso, and F. Casanova, Room-temperature spin Hall effect in graphene/MoS<sub>2</sub> van der Waals heterostructures, *Nano Lett.* **19**, 1074 (2019).
- [38] T. S. Ghiasi, A. A. Kaverzin, P. J. Blah, and B. J. van Wees, Charge-to-spin conversion by the Rashba–Edelstein effect in two-dimensional van der Waals heterostructures up to room temperature, *Nano Lett.* **19**, 5959 (2019).
- [39] L. A. Benítez, W. S. Torres, J. F. Sierra, M. Timmermans, J. H. Garcia, S. Roche, M. V. Costache, and S. O. Valenzuela, Tunable room-temperature spin galvanic and spin Hall effects in van der Waals heterostructures, *Nat. Mater.* **19**, 170 (2020).
- [40] L. Li, J. Zhang, G. Myeong, W. Shin, H. Lim, B. Kim, S. Kim, T. Jin, S. Cavill, B. S. Kim *et al.*, Gate-tunable reversible Rashba-Edelstein effect in a few-layer graphene/2H-TaS<sub>2</sub> heterostructure at room temperature, *ACS Nano* **14**, 5251 (2020).
- [41] A. M. Hoque, D. Khokhriakov, K. Zollner, B. Zhao, B. Karpiaik, J. Fabian, and S. P. Dash, All-electrical creation and control of spin-galvanic signal in graphene and molybdenum ditelluride heterostructures at room temperature, *Commun. Phys.* **4**, 124 (2021).
- [42] M. Offidani, M. Milletari, R. Raimondi, and A. Ferreira, Optimal charge-to-spin conversion in graphene on transition-metal dichalcogenides, *Phys. Rev. Lett.* **119**, 196801 (2017).
- [43] F. Sousa, G. Tatara, and A. Ferreira, Skew-scattering-induced giant antidamping spin-orbit torques: Collinear and out-of-plane Edelstein effects at two-dimensional material/ferromagnet interface, *Phys. Rev. Res.* **2**, 043401 (2020).
- [44] A. Dyrdał, V. K. Dugaev, and J. Barnaś, Spin Hall effect in a system of Dirac fermions in the honeycomb lattice with intrinsic and Rashba spin-orbit interaction, *Phys. Rev. B* **80**, 155444 (2009).
- [45] K. Zollner, S. M. João, B. K. Nikolić, and J. Fabian, Twist- and gate-tunable proximity spin-orbit coupling, spin relaxation anisotropy, and charge-to-spin conversion in heterostructures of graphene and transition metal dichalcogenides, *Phys. Rev. B* **108**, 235166 (2023).
- [46] C. Monaco, A. Ferreira, and R. Raimondi, Spin Hall and inverse spin galvanic effects in graphene with strong interfacial spin-orbit coupling: A quasi-classical Green's function approach, *Phys. Rev. Res.* **3**, 033137 (2021).
- [47] A. Ferreira, Theory of spin-charge-coupled transport in proximitized graphene: an SO(5) algebraic approach, *J. Phys. Mater.* **4**, 045006 (2021).
- [48] A. Ferreira and E. R. Mucciolo, Critical delocalization of chiral zero energy modes in graphene, *Phys. Rev. Lett.* **115**, 106601 (2015).
- [49] M. J. Simão, M. Anđelković, L. Covaci, T. G. Rappaport, J. P. Lopes, and A. Ferreira, KITE: high-performance accurate modelling of electronic structure and response functions of large molecules, disordered crystals and heterostructures, *R. Soc. Open Sci.* **7**, 191809 (2020).
- [50] S. G. de Castro, J. M. V. P. Lopes, A. Ferreira, and D. A. Bahamon, Fast Fourier-Chebyshev approach to real-space simulations of the Kubo formula, *Phys. Rev. Lett.* **132**, 076302 (2024).
- [51] J. H. Garcia, A. W. Cummings, and S. Roche, Spin Hall effect and weak antilocalization in graphene/transition metal dichalcogenide heterostructures, *Nano Lett.* **17**, 5078 (2017).
- [52] A. Dyrdał and J. Barnaś, Spin Hall effect in graphene due to random Rashba field, *Phys. Rev. B* **86**, 161401(R) (2012).
- [53] C. Huang, Y. D. Chong, and M. A. Cazalilla, Direct coupling between charge current and spin polarization by extrinsic mechanisms in graphene, *Phys. Rev. B* **94**, 085414 (2016).
- [54] M. Milletari and A. Ferreira, Quantum diagrammatic theory of the extrinsic spin Hall effect in graphene, *Phys. Rev. B* **94**, 134202 (2016).
- [55] N. M. R. Peres, *Colloquium: The transport properties of graphene: An introduction*, *Rev. Mod. Phys.* **82**, 2673 (2010).
- [56] Z. H. Ni, L. A. Ponomarenko, R. R. Nair, R. Yang, S. Anissimova, I. V. Grigorieva, F. Schedin, P. Blake, Z. X. Shen, E. H. Hill, K. S. Novoselov, and A. K. Geim, On resonant scatterers as a factor limiting carrier mobility in graphene, *Nano Lett.* **10**, 3868 (2010).

- [57] F. Joucken, C. Bena, Z. Ge, E. Quezada-Lopez, S. Pinon, V. Kaladzhyan, T. Taniguchi, K. Watanabe, A. Ferreira, and J. J. Velasco, Direct visualization of native defects in graphite and their effect on the electronic properties of Bernal-stacked bilayer graphene, *Nano Lett.* **21**, 7100 (2021).
- [58] P. Streda, Quantised Hall effect in a two-dimensional periodic potential, *J. Phys. C* **15**, L1299 (1982).
- [59] A. Crépieux and P. Bruno, Theory of the anomalous Hall effect from the Kubo formula and the Dirac equation, *Phys. Rev. B* **64**, 014416 (2001).
- [60] O. V. Dimitrova, Spin-Hall conductivity in a two-dimensional Rashba electron gas, *Phys. Rev. B* **71**, 245327 (2005).
- [61] M. Millettari, M. Offidani, A. Ferreira, and R. Raimondi, Covariant conservation laws and the spin Hall effect in Dirac-Rashba systems, *Phys. Rev. Lett.* **119**, 246801 (2017).
- [62] A. Ferreira, J. Viana-Gomes, J. Nilsson, E. R. Mucciolo, N. M. R. Peres, and A. H. Castro Neto, Unified description of the dc conductivity of monolayer and bilayer graphene at finite densities based on resonant scatterers, *Phys. Rev. B* **83**, 165402 (2011).
- [63] I. A. Ado, I. A. Dmitriev, P. M. Ostrovsky, and M. Titov, Anomalous Hall effect with massive Dirac fermions, *Europhys. Lett.* **111**, 37004 (2015).
- [64] M. Millettari and A. Ferreira, Crossover to the anomalous quantum regime in the extrinsic spin Hall effect of graphene, *Phys. Rev. B* **94**, 201402(R) (2016).
- [65] N. A. Sinitsyn, Q. Niu, and A. H. MacDonald, Coordinate shift in the semiclassical Boltzmann equation and the anomalous Hall effect, *Phys. Rev. B* **73**, 075318 (2006).
- [66] The importance of the unitary regime in graphene-based heterostructures is well understood and can be traced back to the abundance of point defects and resonant scatterers in real systems (see [57,62]).
- [67] See Supplemental Material at <http://link.aps.org/supplemental/10.1103/PhysRevB.109.L241404> for the explicit form of the spin Hall response in the  $i\eta$ -approximation and more details on the use of a momentum cut-off in the numerical calculations of the unitary limit.
- [68] M. Offidani and A. Ferreira, Anomalous Hall effect in 2D Dirac materials, *Phys. Rev. Lett.* **121**, 126802 (2018).
- [69] A. P. Schnyder, S. Ryu, A. Furusaki, and A. W. W. Ludwig, Classification of topological insulators and superconductors in three spatial dimensions, *Phys. Rev. B* **78**, 195125 (2008).
- [70] D. Huertas-Hernando, F. Guinea, and A. Brataas, Spin-orbit-mediated spin relaxation in graphene, *Phys. Rev. Lett.* **103**, 146801 (2009).
- [71] A. Uri, S. Grover, Y. Cao, J. A. Crosse, K. Bagani, D. Rodan-Legrain, Y. Myasoedov, K. Watanabe, T. Taniguchi, P. Moon *et al.*, Mapping the twist-angle disorder and Landau levels in magic-angle graphene, *Nature (London)* **581**, 47 (2020).